PNAS INAUGURAL ARTICLE | PHYSIOLOGY OPEN ACCESS

Protective role of chaperone-mediated autophagy against atherosclerosis

Julio Madrigal-Matute[a,b,1], Jenny de Bruijn[c], Kim van Kuijk[c,d], Dario F. Riascos-Bernal[e], Antonio Diaz[a,b], Inmaculada Tasset[a,b], Adrián Martín-Segura[a,b], Marion J. J. Gijbels[c,f,g], Bianca Sander[c], Susmita Kaushik[a,b], Erik A. L. Biessen[c,h], Simoni Tiano[a,b], Mathieu Bourdenx[a,b], Gregory J. Krause[a,b], Ian McCracken[i], Andrew H. Baker[c,i], Han Jin[c], Nicholas E. S. Sibinga[a,e], Jose Javier Bravo-Cordero[j], Fernando Macian[b,k], Rajat Singh[a,b,e], Patrick C. N. Rensen[l,m], Jimmy F. P. Berbée[l,m,2], Gerard Pasterkamp[n], Judith C. Sluimer[c,i,3,4], and Ana Maria Cuervo[a,b,e,3,4]

This contribution is part of the special series of Inaugural Articles by members of the National Academy of Sciences elected in 2019.

Contributed by Ana Maria Cuervo; received November 23, 2021; accepted February 14, 2022; reviewed by Peter Butler and Toren Finkel

Chaperone-mediated autophagy (CMA) contributes to regulation of energy homeostasis by timely degradation of enzymes involved in glucose and lipid metabolism. Here, we report reduced CMA activity in vascular smooth muscle cells and macrophages in murine and human arteries in response to atherosclerotic challenges. We show that in vivo genetic blockage of CMA worsens atherosclerotic pathology through both systemic and cell-autonomous changes in vascular smooth muscle cells and macrophages, the two main cell types involved in atherogenesis. CMA deficiency promotes dedifferentiation of vascular smooth muscle cells and a proinflammatory state in macrophages. Conversely, a genetic mouse model with up-regulated CMA shows lower vulnerability to proatherosclerotic challenges. We propose that CMA could be an attractive therapeutic target against cardiovascular diseases.

atherosclerotic plaques | lipid challenge | lysosomes | proteolysis | vascular disease

Cardiovascular disease (CVD) is the leading underlying cause of death worldwide, accounting for more than 31.5% of total deaths (1). The main risk factors for the development of atherosclerosis—the most common cause of CV clinical events—such as obesity, hypertension, diabetes, and aging are rising in epidemic proportions due to changes in lifestyle and the growing elderly population (2). In atherosclerosis, hypercholesterolemia leads to vascular endothelial dysfunction and extravasation of atherogenic lipoproteins, resulting in increased adhesion and extravasation of monocytes from the circulation to the intima (3, 4). Once there, monocytes engulf modified low-density lipoproteins (LDLs), differentiate into macrophages and foam cells, and proliferate, forming a neointima with a lipid-laden macrophage core (5). High cytokine secretion and production of nitric oxide (NO) and reactive oxygen species at the lipid-, necrotic-, and macrophage-rich regions create a proinflammatory and oxidative environment that drives dedifferentiation of vascular smooth muscle cells (VSMCs) from a contractile to an activated secretory and migratory phenotype (1, 6–8). Activated VSMCs migrate from the media into the intima, further increasing inflammation, oxidative stress, and collagen and elastin deposition at the fibrous cap (9). The proinflammatory, oxidative, and hypoxic environment in the plaque exacerbates cellular toxicity and cell death and promotes vascular calcification and matrix degradation (10, 11), which together make the plaque prone to rupture and often result in the subsequent clinical event (12).

Autophagy mediates the degradation of cellular components in lysosomes, thus ensuring intracellular quality control and cellular energetics through recycling of essential catabolites (13). Macroautophagy, the most extensively studied type of autophagy, has proven important in endothelial cells (14), VSMCs (15), and macrophages (16) for maintenance of vasculature homeostasis and in response to lipid challenges and protection against atherosclerosis (17). In contrast, the role of other autophagy types in vascular cells is less known. Chaperone-mediated autophagy (CMA) is a selective type of autophagy for proteins bearing a pentapeptide motif (KFERQ-like motif) (18, 19). The heat shock cognate protein (HSC70) recognizes this motif and delivers substrate proteins to lysosome-associated membrane protein type 2A (LAMP-2A), that serves as a receptor and translocation complex upon multimerization (20, 21). Substrate proteins reach the lysosomal lumen through this complex assisted by the lysosomal-resident HSC70 (22–24). Besides removal of oxidized and damaged proteins by CMA, selective and timely degradation of fully functional proteins by this type of autophagy terminates their function. This regulated remodeling of the proteome by CMA is behind its participation in the regulation of multiple intracellular processes, such as glucose and

Significance

Cardiovascular diseases remain the leading cause of death worldwide, with atherosclerosis being the most common source of clinical events. Metabolic changes with aging associate with concurrent increased risk of both type 2 diabetes and cardiovascular disease, with the former further raising the risk of the latter. The activity of a selective type of autophagy, chaperone-mediated autophagy (CMA), decreases with age or upon dietary excesses. Here we study whether reduced CMA activity increases risk of atherosclerosis in mouse models. We have identified that CMA is up-regulated early in response to proatherogenic challenges and demonstrate that reduced systemic CMA aggravates vascular pathology in these conditions. We also provide proof-of-concept support that CMA up-regulation is an effective intervention to reduce atherosclerosis severity and progression.

Competing interest statement: J.M.-M. is a founder and consultant for Instituto Ibions SLP. A.H.B. is a coauthor with T.F. of a review article in 2019. A.M.C. is a cofounder and scientific advisor for the autophagy program at Life Biosciences and consults for Generian Pharmaceuticals and Cognition Therapeutics.

[1]Present address: IBIONS–Instituto Biomédico de Nutrición y Salud, 03600 Elda, Alicante, Spain.

[2]Deceased April 16, 2020.

[3]J.C.S. and A.M.C. contributed equally to this work.

[4]To whom correspondence may be addressed. Email: judith.sluimer@maastrichtuniversity.nl or ana-maria.cuervo@einsteinmed.edu.

This article contains supporting information online at http://www.pnas.org/lookup/suppl/doi:10.1073/pnas.2121133119/-/DCSupplemental.

Published April 1, 2022.

lipid metabolism, cell cycle, transcriptional programs, or T cell activation, among others (25–27). In fact, in vivo blockage of CMA in liver results in exacerbated glycolysis and lipogenesis (25) and blocks lipolysis (26). Although basal levels of CMA are detectable in most mammalian cells, CMA is up-regulated in response to proteotoxicity (28), lipotoxicity (29), oxidative stress (30), and hypoxia (31), all conditions that contribute to the etiology of atherosclerosis (9). Reduced CMA activity—due to lower stability and altered LAMP-2A lysosomal dynamics—has been described upon sustained dietary lipid challenges (high-fat or -cholesterol diets), diabetes, and in aging, all major risk factors for CVD (29, 32–34).

The protective role of CMA against mechanisms related to the etiology of CVD motivated us to investigate the possible contribution of CMA failure to the development of atherosclerosis (35). Here, we show that blockage of CMA in mice increases their vulnerability to proatherosclerotic challenges, through both systemic and cell-autonomous changes in VSMCs and macrophages, the two main cell types involved in atherogenesis. Loss of CMA in VSMCs promotes their dedifferentiation and higher susceptibility to lipid challenges, while defective CMA in macrophages leads to a more proinflammatory phenotype. We propose that CMA is a defense mechanism activated in the vasculature in response to proatherosclerotic challenges and that reduced CMA activity leaves the vasculature vulnerable to these challenges. Using mice with genetically enhanced CMA, we demonstrate that, when exposed to proatherosclerotic challenges, they display reduced disease severity and slower progression. Our findings support that CMA could be a therapeutic target for atherosclerosis.

Results

CMA Blockage Exacerbates Atherosclerosis in a Murine Experimental Model. We used the recently developed transgenic mouse model expressing a fluorescent reporter for CMA (KFERQ-PS-Dendra2 mice) that allows measuring CMA activity in vivo (36) to determine the status of CMA in the vasculature and its possible changes during atherosclerotic plaque development. When the KFERQ-PS-Dendra CMA substrate is delivered to lysosomes, CMA activity is detected as fluorescent puncta against the diffuse fluorescent cytosolic pattern (36). Using aortas from healthy mice and two-photon microscopy in fixed tissue or intravital two-photon microscopy, we found fluorescent puncta in cells in the media (VSMCs) and to less extent in the intima (endothelial cells) (Fig. 1 *A* and *B* and *SI Appendix*, Fig. S1*A*). Injection of fluorescent dextran that highlights the lysosomal compartment upon internalization from the bloodstream by endocytosis demonstrated colocalization with the Dendra signal in a fraction of lysosomes, in support of active CMA in the vasculature under basal conditions (Fig. 1*C*). When we promoted atherosclerosis development in KFERQ-PS-Dendra2 mice through hypercholesterolemia (using injection of adeno-associated virus 8–mediated overexpression of proprotein convertase subtilisin/kexin type 9 [AAV8-PCSK9] and a high cholesterol–containing diet [Western-type diet; WD] for 12 wk), aortas from these mice revealed a marked reduction in the number of fluorescent puncta that was almost absent in the plaque (Fig. 1 *D* and *E* and *SI Appendix*, Fig. S1*B* show maximal projections throughout the plaque area, with collagen highlighted in red). Costaining of these atherosclerotic aortas with the VSMC marker α-smooth muscle actin (αSMA) and the macrophage marker cluster of differentiation 68 (CD68) revealed almost no CMA activity in either cell type (*SI Appendix*, Fig. S1*C*). Immunohistochemistry of the plaque demonstrated that levels of LAMP-2A, the limiting component for CMA, can be detected both in VSMCs and macrophages by 6 wk of plaque formation, but LAMP-2A levels significantly decreased in more advanced stages (12 wk) of murine atherosclerotic disease in both VSMCs and macrophages, in agreement with the observed reduction in CMA activity (Fig. 1*F* and *SI Appendix*, Fig. S1*D*).

To determine if the initial up-regulation of LAMP-2A in response to the dietary challenge was protective and whether reduced CMA contributes to disease progression, we used a mouse model with systemic blockage of CMA [constitutive knockout for LAMP-2A; L2AKO (37)] (*SI Appendix*, Fig. S1*E*). At 3 mo of age, L2AKO mice on chow diet display slightly lower body weight and circulating total cholesterol levels than wild-type (WT) littermates (*SI Appendix*, Fig. S1 *F* and *G*). When L2AKO mice were fed WD for 12 wk, we observed a marked increase in total circulating cholesterol and triglyceride (TG) levels (Fig. 1 *G* and *H*), mainly in the very-low-density lipoprotein (VLDL) and LDL fractions (Fig. 1 *I* and *J*). Atherosclerotic plaques in the aortic root of L2AKO mice were larger than in WT mice (~39%) (Fig. 1 *K* and *L*), with a noticeable trend towards bigger necrotic cores, lower cellularity, and significantly more advanced plaques (Fig. 1 *M* and *N* and *SI Appendix*, Fig. S1*H*). Plaques in the CMA-incompetent mice also had more collagen content and a thicker fibrous cap yet a higher abundance of calcifications (Fig. 1 *O*–*R* and *SI Appendix*, Fig. S1*I*). In addition, the relative contents of both αSMA for contractile VSMCs and CD68+ for macrophages in the plaque were significantly lower in L2AKO mice (Fig. 1 *S* and *T*).

Overall, reduced CMA activity associates with many aspects of more severe atherosclerotic pathology, supporting an antiatherosclerotic protective function for CMA.

Metabolic Dysfunction in CMA-Deficient Mice. To determine the basis for the protective effect of CMA against atherosclerosis and because of the previously described regulation of hepatic glucose and lipid metabolism by CMA (25), we evaluated metabolic parameters shown to be major risk factors for CVD. We found that L2AKO mice gained 50% more body weight than the WT group during the 12 wk of WD (Fig. 2*A*), mostly due to a higher fat mass content (Fig. 2*B* and *SI Appendix*, Fig. S2*A*). Indirect calorimetry revealed that the increased adiposity of L2AKO mice did not originate from higher food consumption (Fig. 2*C* and *SI Appendix*, Fig. S2 *B* and *C*), but could be explained by reduced energy expenditure (Fig. 2*D* and *SI Appendix*, Fig. S2 *D* and *E*) and less physical activity (Fig. 2*E*). The decrease in respiratory exchange ratio (RER)—indicative of lipid use as energy—observed in WT mice on WD was significantly more pronounced in L2AKO mice (*SI Appendix*, Fig. S2*F*), suggesting impaired carbohydrate utilization in these mice. Indeed, L2AKO mice showed marked hyperinsulinemia (Fig. 2*F*) and increased insulin resistance (Fig. 2 *G* and H), typical risk factors for CVD (38). Circulating levels of the prothrombotic and profibrotic cytokine plasminogen activator inhibitor type 1 (PAI-1) were also significantly higher in L2AKO mice (Fig. 2*I*). These findings support that loss of CMA accentuates the systemic derangements in metabolism and coagulation imposed by the WD, thus rendering organisms more prone to atherosclerosis.

CMA Blockage Promotes VSMC Dedifferentiation. Whereas circulating cholesterol levels in WT mice show the previously described correlation with different plaque properties, such

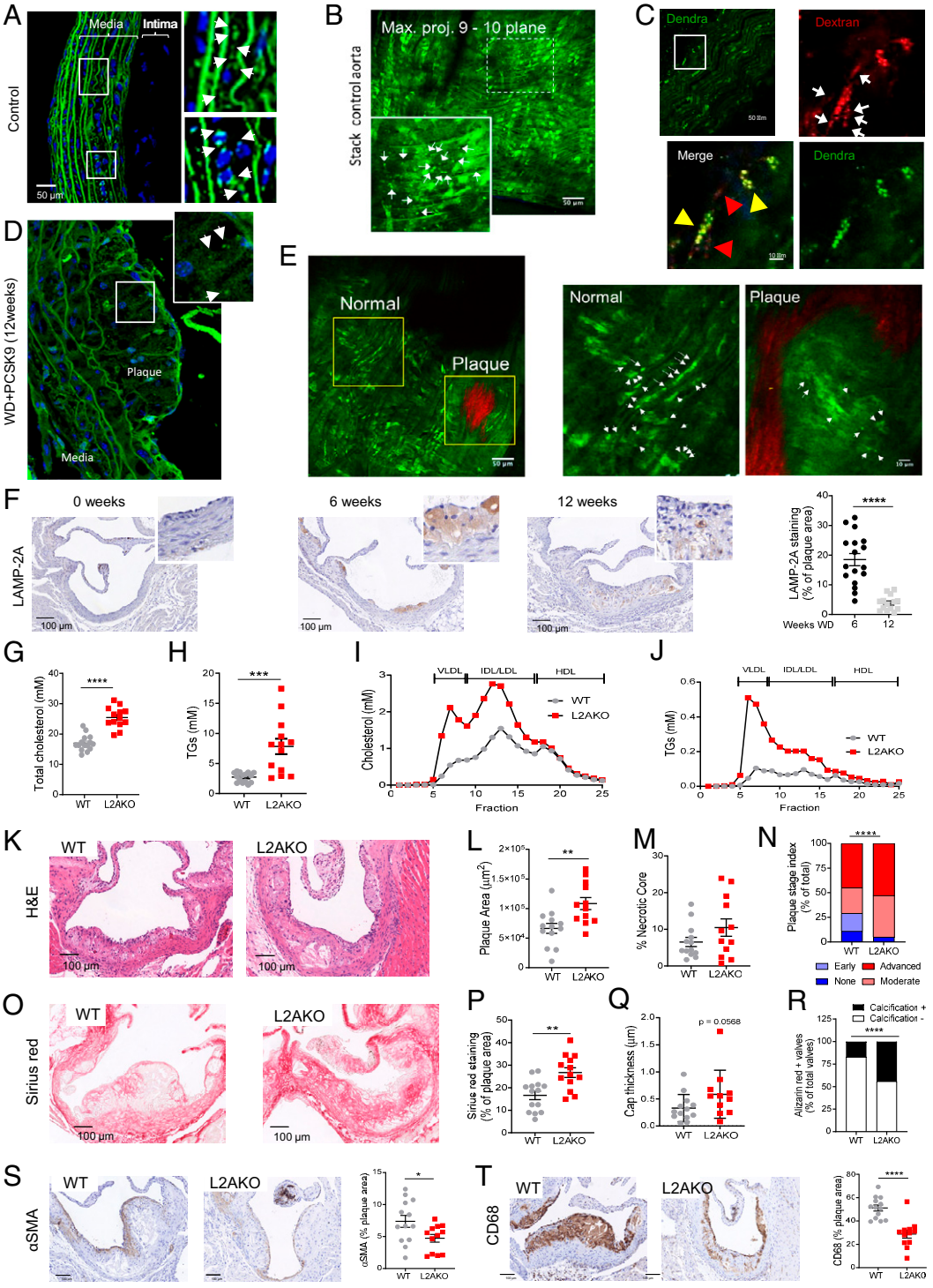

Fig. 1. CMA deficiency aggravates atherosclerosis in a murine experimental model. (*A–E*) CMA activity in aorta from KFERQ-Dendra2 mice untreated (Control; *A–C*) or subjected to a proatherosclerotic treatment (injected with AAV8-PCSK9 and maintained for 12 wk on WD; *D* and *E*). (*A–E*, *Insets*) Boxed areas at higher magnification. Arrows indicate fluorescent puncta. In *C*, animals were injected with fluorescent dextran (in red) to highlight endolysosomal compartments. Individual and merged channels of the boxed regions at higher magnification are shown. Arrowheads indicate dextran+Dendra+ puncta (yellow) and dextran+ only puncta (red). Collagen (red) was visualized by second harmonic generation (*E*). (*F*) Levels of LAMP-2A at the indicated times of the proatherosclerotic intervention. Representative images of aorta sections (*Left*) and quantification in the neointima (*Right*); $n = 18$. (*G–J*) Circulating lipids in WT and LAMP-2A–null mice (L2AKO) subjected to the proatherosclerotic challenge for 12 wk. (*G–J*) Circulating total cholesterol (*G*), TGs (*H*), cholesterol profile (*I*), and TG profile (*J*). Individual values (*G* and *H*) and average curves (*I* and *J*) are shown; ($n = 15$ WT, $n = 14$ L2AKO). (*K–T*) Plaque properties in the same mouse groups. Representative images of aortas stained for hematoxylin and eosin (H&E) (*K*) or sirius red (*O*) and quantification of plaque area (*L*), size of the necrotic core (*M*), plaque stage index (*N*), sirius red–positive area (*P*), and cap thickness (*Q*). Calcification analysis in aortas stained for alizarin red (*R*) as shown in *SI Appendix*, Fig. S1*I* . (*S* and *T*) Representative images of aortas immunostained for αSMA (VSMCs) (*S*) and CD68 macrophages (*T*) and quantification of the stained area (*Right*); ($n = 13$ WT, $n = 12$ L2AKO). Individual values (symbols) and mean ± SEM are shown. Experiments in *A–E* were repeated three times with similar results. All data were tested for normal distribution using the D'Agostino and Pearson normality test. Variables that did not pass the normality test were subsequently analyzed using the Mann–Whitney *U* rank-sum test. All other variables were tested with the Student's *t* test. $*P < 0.05$, $**P < 0.01$, $***P < 0.005$, and $****P < 0.0001$.

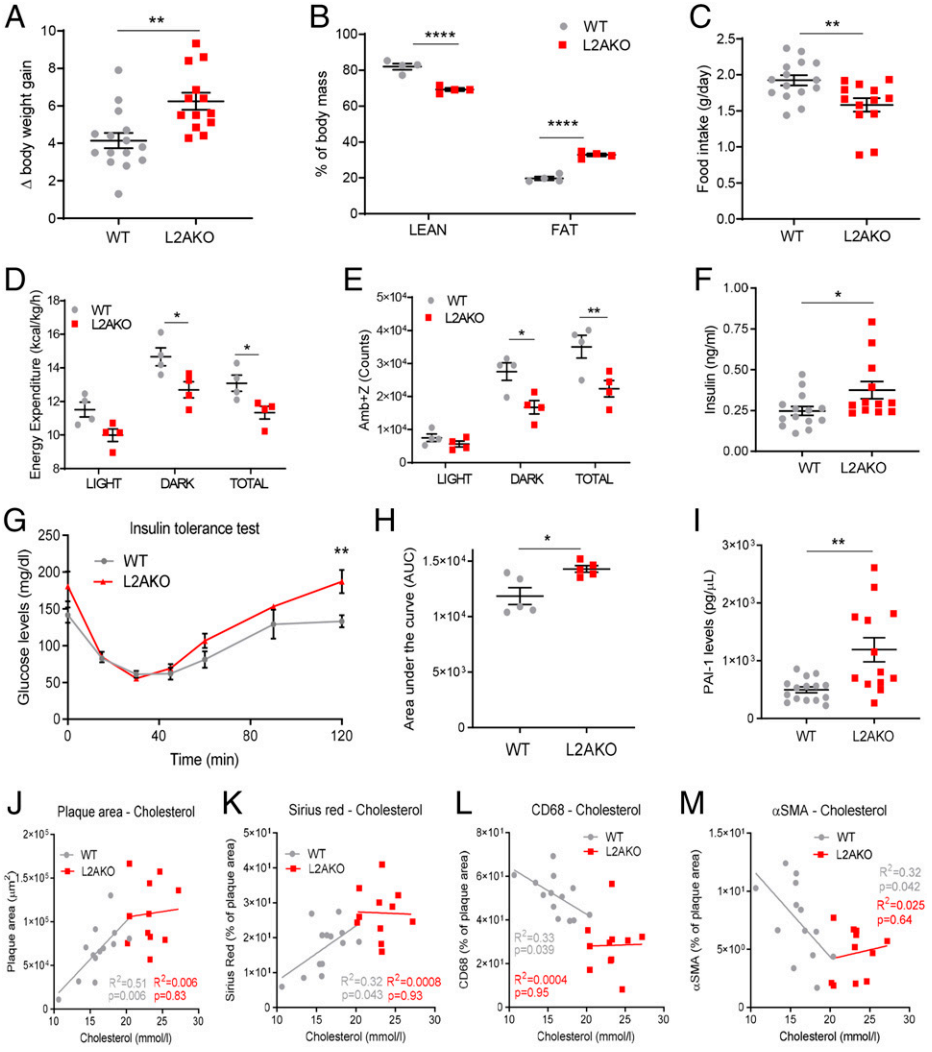

Fig. 2. Proatherogenic challenge elicits metabolic dysfunction in CMA-deficient mice. (*A–E*) WT and L2AKO mice subjected to a proatherosclerotic treatment (injected with AAV8-PCSK9 and maintained for 12 wk on WD) were compared for body weight gain (n = 15 WT, n = 14 L2AKO) (*A*), body composition (n = 4) (two-way ANOVA, F = 120.1; P < 0.0001 for interaction, F = 1736; P < 0.0001 for lean/fat, F = 0.01544; P = 0.9032 for genotype; n = 4) (*B*), food intake (n = 14 WT, n = 16 L2AKO) (*C*), energy expenditure (two-way ANOVA, F = 0.1185; P = 0.8889 for interaction, F = 21.05; P < 0.0001 for light/dark/total, F = 22.41; P = 0.0002 for genotype; n = 4) (*D*), and ambulatory parameters (x + z axes) (two-way ANOVA, F = 3.194; P = 0.0650 for interaction, F = 49.75; P < 0.0001 for light/dark/total, F = 20.75; P = 0.0002 for genotype; n = 4) (*E*). (*F–I*) Circulating levels in the same mouse groups of insulin (n = 15 WT, n = 14 L2AKO) (*F*), glucose during an insulin tolerance test (repeated-measures two-way ANOVA after Bonferroni's post hoc test, F = 1.851; P = 0.1090 for interaction, F = 31.96; P < 0.0001 for time, F = 15.99; P = 0.0040 for genotype; n = 5) (*G*), area under the curve from the insulin tolerance test (*H*), and circulating PAI-1 levels (n = 15 WT, n = 14 L2AKO) (*I*). (*J–M*) Correlation between plasma cholesterol and different plaque parameters: plaque area (*J*), collagen (*K*), macrophages (*L*), and % VSMC of plaque area (*M*) in the same mouse groups (n = 15 WT, n = 14 L2AKO). All data, when applicable, were tested for normal distribution using the D'Agostino and Pearson normality test. Variables that did not pass the normality test were subsequently analyzed using the Mann–Whitney U rank-sum test. All other variables were tested with the Student's t test. Individual values (symbols) and mean ± SEM are shown. *P < 0.05, **P < 0.01, and ****P < 0.001.

correlations are lost in L2AKO mice (Fig. 2 *J–M*). This suggests that factors other than systemic metabolic changes also contribute to the higher vulnerability of L2AKO mice to atherosclerosis. This motivated us to investigate whether local changes of CMA in the vasculature could contribute to disease progression.

We first examined CMA in primary cultured VSMCs exposed to a physiological lipid challenge (LDL loading) and found a dose-dependent up-regulation of CMA followed by a gradual decrease once toxic concentrations of LDL are reached (Fig. 3*A* and *SI Appendix*, Fig. S3*A*). Exposure of L2AKO VSMCs (*SI Appendix*, Fig. S3*B*) to fluorescent LDL (diLDL) resulted in higher intracellular lipid accumulation (Fig. 3*B*) and reduced cellular viability as LDL concentrations increased (Fig. 3*C*). This higher susceptibility to lipotoxicity can be primarily attributed to the loss of CMA, since other types of autophagy (i.e., macroautophagy, shown in *SI Appendix*, Fig. S3 *C–F*) were fully functional in these cells.

Comparative analysis of the transcriptional profile of WT and L2AKO VSMCs revealed marked differences under basal conditions and an inadequate transcriptional response after exposure to LDL in L2AKO cells (Fig. 3*D* and *SI Appendix*, Fig. S4 *A–C*). Under basal conditions, L2AKO VSMCs exhibited loss of *Acta2*, an activated macrophage–like gene profile, and acquisition of recently identified markers of modified, dedifferentiated VSMCs (8) (Fig. 3*D* and *SI Appendix*, Fig. S4*D*). These findings are in line with loss of ACTA2+ contractile SMCs in the plaques in vivo (Fig. 1*S*). Gene set enrichment analysis (with the STRING database) further showed up-regulation of nodes related to cell migration, proliferation, differentiation, and response to lipids (*SI Appendix*, Fig. S4*E*).

Loading with LDL induced changes in genes related to lipid metabolism in both genotypes (*SI Appendix*, Fig. S4*F*), but we identified quantitative differences in this response. Thus, using Ingenuity Pathway Analysis (IPA), we found that L2AKO cells have a defective response to the lipid challenge with reduced up-regulation of genes involved in the cholesterol pathway and display cholesterol as one of the top molecules up-regulated in these cells, in line with the in vivo data (Fig. 1*G* and *SI Appendix*, Fig. S4*G*). The immune component of the response of VSMCs to lipids is also different in L2AKO cells. While WT cells orchestrate a well-characterized inflammatory response, the immune response of L2AKO cells is mainly composed of genes related to leukocyte activation and cell migration (*SI Appendix*, Fig. S4*F*). Differential gene expression analysis and gene set enrichment upon lipid loading also identified gene nodes unique for L2AKO cells related to cell death and cellular response to stress, including the response to DNA damage (Fig. 3*E*), which we experimentally confirmed to be significantly increased in these cells (Fig. 3 *F* and *G*). These findings support that failure to activate CMA in VSMCs makes them unable to adapt to the environmental lipid challenge, as previously also described in CMA-deficient hepatocytes (25).

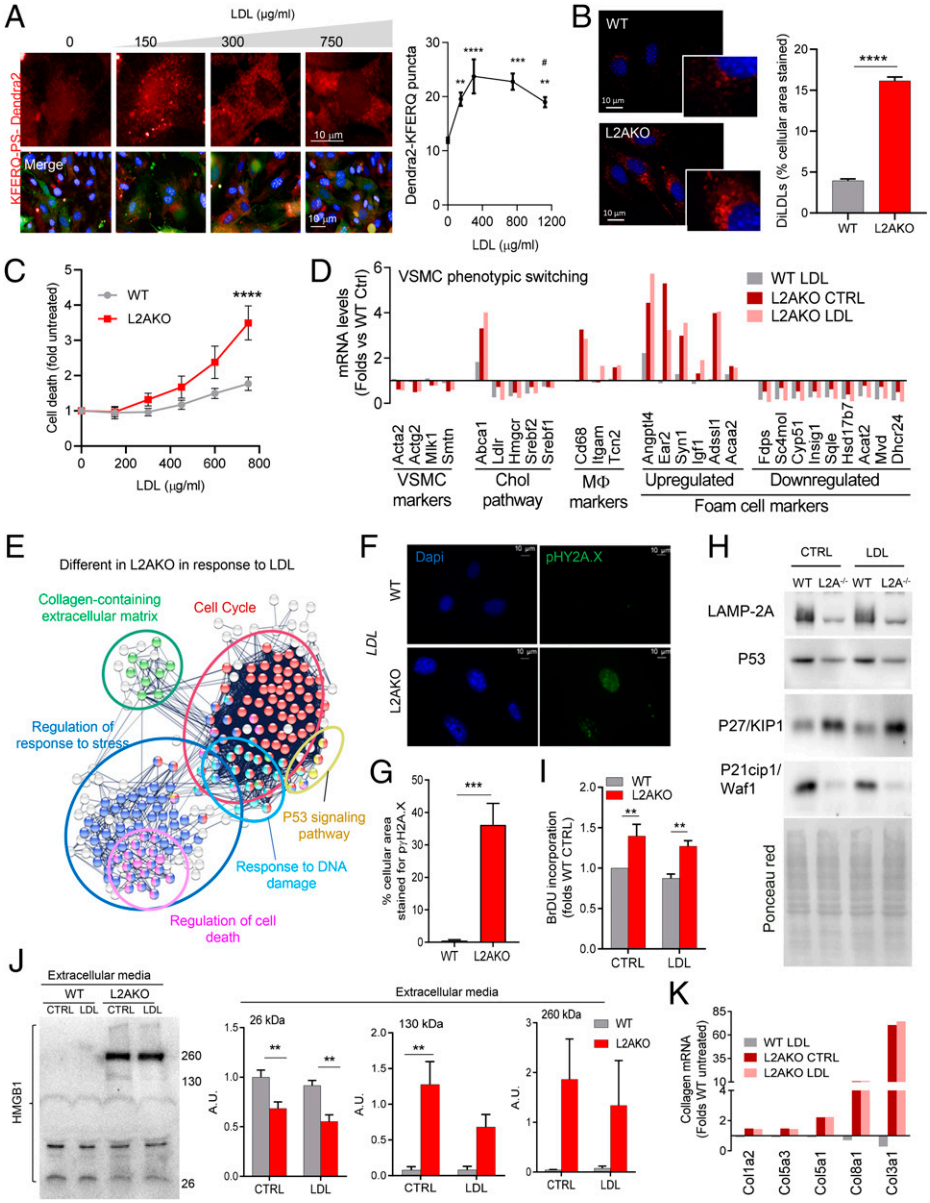

Fig. 3. CMA blockage makes VSMCs vulnerable to lipotoxicity and promotes their dedifferentiation. (*A*) CMA activity in VSMCs stably expressing the KFERQ-PS-Dendra2 CMA reporter and exposed to increasing concentrations of LDL. Representative images (*Left*) of red channel (*Top*) or merged channels (*Bottom*). Nuclei are highlighted with DAPI. Quantification of CMA activity as the average number of fluorescent puncta per cell using high-content microscopy (n > 2,500 cells per condition in six different wells and three independent experiments). Statistically significant differences compared with basal (*) or between groups with LDL ($^{\#}$) were analyzed by one-way ANOVA with Tukey's post hoc test (**P < 0.005, ***P = 0.001, ****P < 0.0001, and $^{\#}P$ < 0.05). (*B*) Intracellular levels of diLDL-derived fluorescence in VSMCs from WT and L2AKO mice. Representative images (*Left*) and quantification (*Right*) (n = 3, >45 cells per experiment in three different experiments). (*B, Insets*) Higher magnification. (*C*) Cytotoxicity in the same cells in response to increasing concentrations of LDL (two-way ANOVA after Bonferroni's post hoc test, F = 2.862; P = 0.9872 for interaction, F = 2.205; P = 0.1570 for LDL concentration, F = 21.93; P = 0.0002 for genotype; n = 4-5). (*D*) Changes in mRNA levels of different markers of cell identity, macrophage-related, and cholesterol pathway in the same VSMCs stimulated with LDL or maintained in medium with delipidated fetal bovine serum (LPDS) (CTRL) (pool of three individual experiments). (*E*) STRING analysis for pathways differentially regulated in L2AKO cells in response to LDL compared with control (pool of three individual experiments). (*F* and *G*) Representative images (*F*) and quantification (*G*) of immunofluorescence for pγH2A.X in WT and L2AKO primary VSMCs after LDL loading (n = 3, >5 cells per experiment). (*H*) Immunoblot for components of the P53 signaling pathway in WT and L2AKO (L2A$^{-/-}$) VSMCs in basal conditions and upon LDL loading. Ponceau red staining is shown as loading control. The experiment was repeated four times with similar results. (*I*) Bromodeoxyuridine (BrDU) incorporation in WT and L2AKO primary VSMCs in basal conditions and upon LDL loading (two-way ANOVA after Bonferroni's post hoc test, F = 0.0002639; P = 0.0183 for interaction, F = 19.35; P < 0.0001 for cells with/without LDL, F = 19.61; P < 0.0001 for genotype; n = 5). (*J*) Immunoblot (*Left*) for HMGB1 in the culture media of WT and L2AKO primary VSMCs in basal conditions and upon LDL loading. Quantification (*Right*) (in arbitrary densitometric units; A.D.U.) of the indicated molecular mass variants of HMGB1 (26 kDa: two-way ANOVA after Bonferroni's post hoc test, F = 0.1301; P = 0.7246 for interaction, F = 2.801; P = 0.1201 for cells with/without LDL, F = 27.50; P = 0.0002 for genotype; 130 kDa: two-way ANOVA after Bonferroni's post hoc test, F = 2.578; P = 0.1343 for interaction, F = 2.516; P = 0.1387 for cells with/without LDL, F = 23.19; P = 0.0004 for genotype; 260 kDa: two-way ANOVA after Bonferroni's post hoc test, F = 0.2109; P = 0.6543 for interaction, F = 0.1635; P = 0.6930 for cells with/without LDL, F = 6.462; P = 0.0258 for genotype; n = 4). (*K*) Changes in mRNA levels of the main collagen genes in primary WT and L2AKO VSMCs stimulated with LDL or maintained in medium with LPDS (CTRL) (pool of three individual experiments). All data, when applicable, were tested for normal distribution using the D'Agostino and Pearson normality test. Variables that did not pass the normality test were subsequently analyzed using the Mann–Whitney U rank-sum test. All other variables were tested with the Student's t test. Values are mean ± SEM. **P < 0.01, ***P < 0.005, and ****P < 0.001.

Analysis of upstream regulators of the group of genes differentially expressed in L2AKO VSMCs revealed as the top change a significant ($P < 3.13 \times 10^{-46}$) down-regulation of the tumor protein 53 (P53) signaling pathway (Fig. 3*E*). Immunoblot against different components of the P53 signaling pathways confirmed markedly reduced levels of P53 protein

and of the cyclin-dependent kinase inhibitor 1A (P21) in L2AKO VSMCs, whereas cyclin-dependent kinase inhibitor 1B (P27) content was higher in these cells compared with WT (Fig. 3*H*). In light of the well-characterized role of P53 as an antiapoptotic molecule in response to lipid challenges, the identified a defect in P53 signaling in L2AKO VSMCs provides an explanation for their higher death count (Fig. 3*C*), increased DNA damage (Fig. 3 *F* and *G*), and higher proliferation rates (Fig. 3*I*) upon LDL loading. Furthermore, relevant to this study is the fact that P53 has previously been shown to protect against VSMC dedifferentiation (39), a transcriptional pattern already noticeable in L2AKO VSMCs under basal conditions (Fig. 3*D*).

We also detected that L2AKO VSMCs show constitutively higher intracellular content of the proinflammatory and damage/danger-associated molecule pattern chaperone high mobility group box protein-1 (HMGB1) (*SI Appendix*, Fig. S4*H*), known to complex with P53 (40, 41) and to stimulate PAI-1 (42). Even more striking was the augmented release of HMGB1 into the extracellular media in the form of large–molecular mass complexes (Fig. 3*J*). This continuous release of HMGB1 from L2AKO VSMCs in the arterial wall may be one of the major drivers of the local inflammation and calcium deposition observed in the aortas of L2AKO mice (Fig. 1*R* and *SI Appendix*, Fig. S1*I*) and may also contribute to perpetuate dedifferentiation of CMA-defective VSMCs. Also, as part of the possible impact of L2AKO VSMCs in the arterial wall and in agreement with our in vivo observations (Fig. 1 *O* and *P*), we found a marked increase in most of the collagen genes previously associated with plaque fibrosis (Fig. 3*K*), which further supports VSMC transition into a synthetic phenotype.

Our findings in L2AKO VSMCs confirm that fully functional CMA is required in their defense against lipotoxicity and to maintain the identity of VSMCs by preventing their dedifferentiation into secretory–migratory cells.

Proinflammatory Phenotype of CMA-Defective Macrophages. The presence of macrophages in the plaque and their associated inflammatory phenotype influence plaque fate. Therefore, we next set out to investigate the consequences of CMA blockage in macrophage function using in vitro protocols for polarization of bone marrow–derived macrophages (BMDMs) to mimic the plaque proinflammatory phenotype of these cells (interferon γ plus lipopolysaccharide; IFNγ+LPS). We found that CMA-defective BMDMs, when stimulated with IFNγ+LPS, show a stronger proinflammatory profile (higher inducible nitric oxide synthase [iNOS] and cytochrome *c* oxidase 2 [COX2] levels; Fig. 4 *A*–*C* and *SI Appendix*, Fig. S5 *A* and *B*), suggesting that CMA may modulate proinflammatory polarization of macrophages. Interestingly, although the changes in COX2 levels were in large part due to its transcriptional up-regulation, in the case of iNOS the increase was only at the level of protein, in support of changes in protein degradation contributing to the observed elevated cellular iNOS levels (Fig. 4 *A*–*C*). We did not observe differences in macroautophagic activity between WT and L2AKO BMDMs (*SI Appendix*, Fig. S5*C*), in support of the observed phenotype being primarily a consequence of loss of CMA.

We aimed to identify the subset of the proteome that, by not undergoing degradation through CMA, could be behind this exacerbated inflammatory phenotype seen in the L2AKO BMDMs. Thus, we isolated the pool of lysosomes usually active for CMA, those that contain high levels of luminal HSC70, from WT and L2AKO BMDMs, untreated (control; CTRL) or stimulated with IFNγ+LPS. In half of the cultures, we inhibited lysosomal proteolysis to discriminate proteins undergoing degradation inside lysosomes from lysosomal resident proteins (Fig. 4*D* and *SI Appendix*, Fig. S5*D*) and subjected the samples to comparative quantitative proteomics (25). About 45% of the proteins were constitutive lysosomal components, not degraded in lysosomes in resting or stimulated BMDMs (Fig. 4*E*). CMA substrates are defined as those proteins undergoing degradation in lysosomes in a LAMP-2A–dependent manner (Fig. 4*D* and *SI Appendix*, Fig. S5 *E* and *F*). Stimulation with IFNγ+LPS resulted in an increase of lysosomal protein degradation, mostly of CMA substrates (46% increase in CMA substrates vs. only 15% increase in non-CMA lysosomal substrates; Fig. 4*F*). In addition, the repertoire of CMA substrates degraded by untreated and stimulated BMDMs was largely different, with only 7% coinciding proteins (Fig. 4*G*). Data mining using STRING and IPA with the subset of proteins that fail to undergo degradation in unstimulated L2AKO BMDM identified that the top cellular pathways were related to regulation of the immune response, cell-adhesion molecules, and leukocyte activation, besides the expected up-regulation of the proinflammatory LPS signaling pathway (Fig. 4*H* and *SI Appendix*, Fig. S5*G*). The IFNγ+LPS treatment induced CMA degradation of NOS along with five other stimulators of NO synthesis (Fig. 4*I*), which can explain the higher levels of iNOS in CMA-incompetent macrophages upon stimulation (Fig. 4 *A* and *B*). CMA substrates in this condition also included proteins involved in the immune response, neutrophil degradation, and transendothelial migration (including cell adhesion, cellular localization, and interaction with the vascular wall) (Fig. 4*J* and *SI Appendix*, Fig. S5*H*). The in vivo data confirmed these findings, since we found that L2AKO mice showed marked monocytosis, mainly derived from a higher number of proinflammatory monocytes (Fig. 4 *K* and *L*), and an elevated number of T cells, especially CD4+ T cells (Fig. 4 *M* and *N* and the full blood leukocyte pattern in the same mice shown in *SI Appendix*, Table S1).

Overall, our findings support that CMA contributes to the remodeling of the proteome induced by macrophage stimulation, and that defective CMA in these cells promotes a more proinflammatory phenotype.

Human Carotid CMA Response to Proatherosclerotic Conditions. Our in vitro and in vivo findings support that CMA up-regulation may be part of the vascular response to proatherosclerotic challenges. To test whether that was also the case in human atherosclerosis, we have used four different human datasets (clinical characteristics for the different human cohorts in this section are described in *SI Appendix*, *Methods* and *SI Appendix*, Tables S2 and S3). We first confirmed the presence of the CMA receptor in plaque VSMCs and macrophages using costaining for LAMP-2A and αSMA/CD68 (Fig. 5 *A* and *B*; see details in *SI Appendix*, *Methods*, study 1). Analysis of levels of LAMP-2A in human autopsy-derived atherosclerotic plaques from asymptomatic patients at different plaque stages revealed that LAMP-2A levels at the plaque increase gradually with disease progression (graded as plaques with moderate intimal thickening [IT], pathological intimal thickening [PIT], thick fibrous cap atheroma [TkFCA], and intraplaque hemorrhage [IPH]) (Fig. 5 *C* and *D*). Similarly, *LAMP*-2A messenger RNA (mRNA) levels in carotid plaques, surgically retrieved from symptomatic patients (from ref. 43; see details in *SI Appendix*, *Methods*, study 2), directly correlated with the size of the plaque but not the necrotic core (Fig. 5 *E* and *F*). To determine the

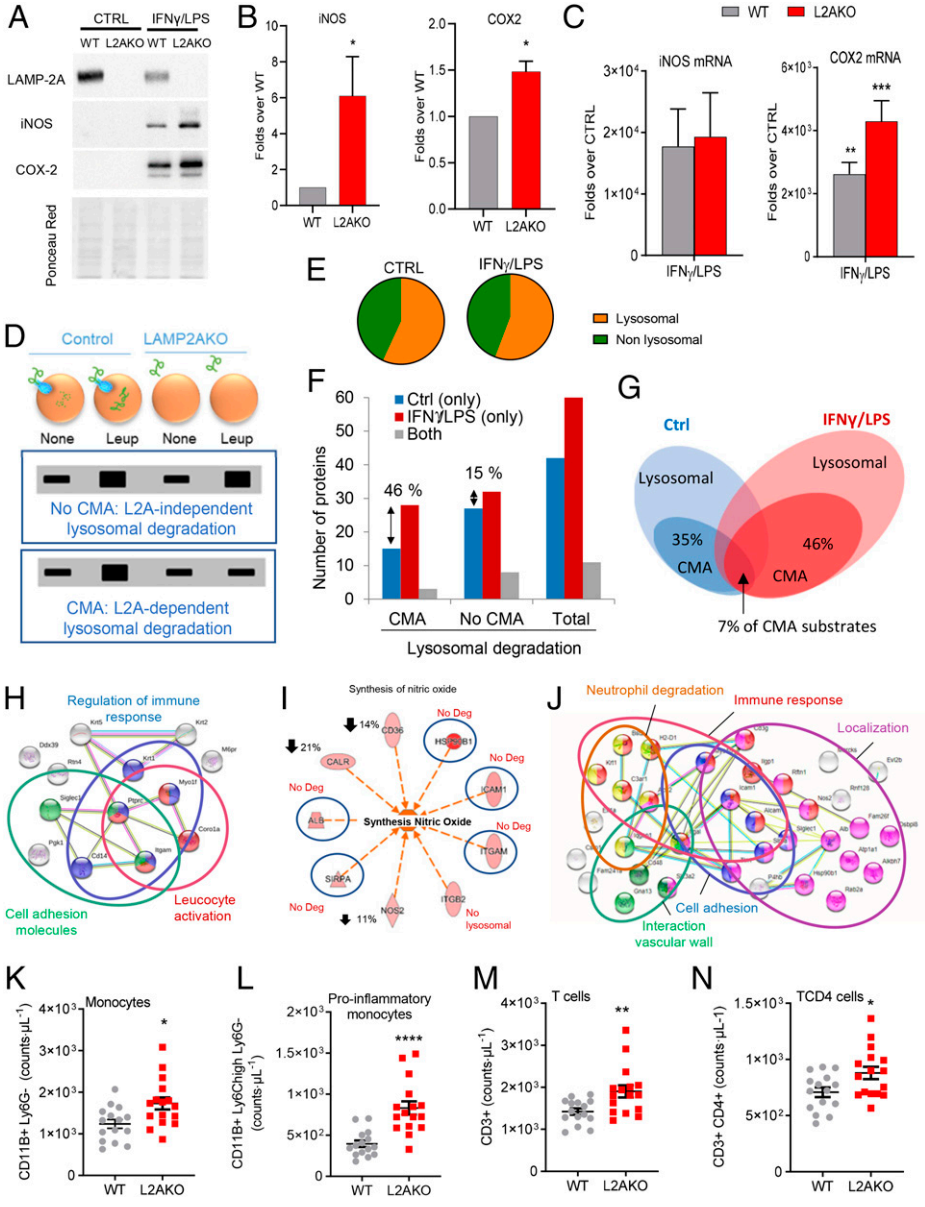

Fig. 4. CMA blockage leads to an exacerbated proinflammatory phenotype in macrophages. (*A* and *B*) Levels of iNOS and COX2 proteins in BMDMs from WT and L2AKO mice cultured without additions (CTRL) or stimulated with IFNγ+LPS. Representative immunoblot (*A*) and densitometric quantification (*B*) expressed as folds over WT levels (n = 5 iNOS, n = 3 COX2). Ponceau red is shown as loading control. (*C*) mRNA levels of iNOS and Cox2 in the same cells expressed as folds over untreated (CTRL) (n = 4 iNOS, n = 3 Cox2). (*D–J*) Comparative proteomic analysis of lysosomes isolated from untreated (none) or leupeptin-treated WT and L2AKO BMDMs untreated (CTRL) or exposed to IFNγ+LPS from a pool of three individual experiments. Schematic of the experimental design and anticipated results for hypothetical proteins undergoing CMA-dependent or -independent lysosomal degradation (*D*). Percentage of lysosomal (constituents) and nonlysosomal proteins (substrates) in the fractions from CTRL and IFNγ+LPS macrophages (*E*). Number (*F*) and percentage (*G*) of proteins undergoing lysosomal degradation (Total) in a LAMP-2A–dependent (CMA) or -independent (no CMA) manner. STRING analysis for the top intracellular networks of CMA substrates in CTRL (*H*) and IFNγ+LPS (*J*) BMDMs. Detail of changes in degradation of proteins involved in synthesis of NO (*I*); blue circles indicate proteins no longer degraded in lysosomes in the L2AKO group, and down arrows indicate the reduction in lysosomal degradation of those proteins in the same group. (*K–N*) Number of total monocytes (*K*), proinflammatory subtype of monocytes (*L*), total T cells (*M*), and TCD4 cells (*N*) in WT and L2AKO mice (n = 15 WT, n = 16 L2AKO). All data, when applicable, were tested for normal distribution using the D'Agostino and Pearson normality test. Variables that did not pass the normality test were subsequently analyzed using the Mann–Whitney U rank-sum test. All other variables were tested with the Student's t test. All values are mean ± SEM. Individual values are shown also in *K–N*. *P < 0.05, **P < 0.01, ***P < 0.005, and ****P < 0.001.

cell type mainly contributing to the elevated levels of *LAMP-2A* in the plaque, we analyzed the correlation between *LAMP-2A* mRNA levels and different cell types and found a direct correlation between LAMP-2A and CD68, a marker of macrophages and foam cells, in human atherosclerotic plaques (Fig. 5 *G* and *H*). We interpreted these changes in LAMP-2A levels as an attempt of the plaque cells, mostly macrophages, to up-regulate this autophagic pathway in response to the proatherosclerotic changes prior to clinical events, as we observed in the experimental mouse model (Fig. 1*D*). In fact, holistic analysis of the CMA transcriptional network using single-cell RNA sequencing (scRNAseq) from human coronary atherosclerotic plaques (from ref. 8; details in *SI Appendix*, *Methods*, study 3) confirmed macrophages as the cells with the highest expression of CMA effectors (*LAMP-2A* and *HSC70*) when compared with endothelial and smooth muscle cells from the same plaques (Fig. 5*I* and *SI Appendix*, Fig. S6 *A* and *B*).

To evaluate possible changes of CMA after the clinical event, we performed immunoblotting for LAMP2 in carotid segments retrieved from surgery in patients who suffered one event at baseline or an additional clinical vascular event at follow-up (44) (see details in *SI Appendix*, *Methods*, study 4 and *SI Appendix*, Tables S2 and S3). This revealed a significant decrease in LAMP2 levels in carotid segments from all patients who developed a second event (Fig. 5*J*). This decrease in LAMP2 seems to be driven mostly by the female patients in this group, who were the ones displaying the most pronounced changes in overall LAMP2 content (Fig. 5*K* and *SI Appendix*, Fig. S6 *C* and *D*). Changes cannot be attributed to differences in patients' ages that were 66.1 ± 3.4 and 70.4 ± 3.8 y for the first and second event, respectively, in female patients and 65.6 ± 1.3 and 74.3 ± 1.2 y for the same groups in male patients. Indeed, sex-stratified logistic regression confirmed a significant association of LAMP-2A with an additional clinical event and with time to event in women (n = 22), independent of age, body mass index (BMI), or hypertension, but not in men (n = 37; *SI Appendix*, Tables S4 and S5). Although this study is not sufficiently powered to discard other cofounding effects, we did not find direct correlations of LAMP2 levels and any of the available clinical parameters (*SI Appendix*, Fig. S6 *F–J*). The observed changes seem selective for LAMP2, rather than an overall reduction in the lysosomal content, since levels of

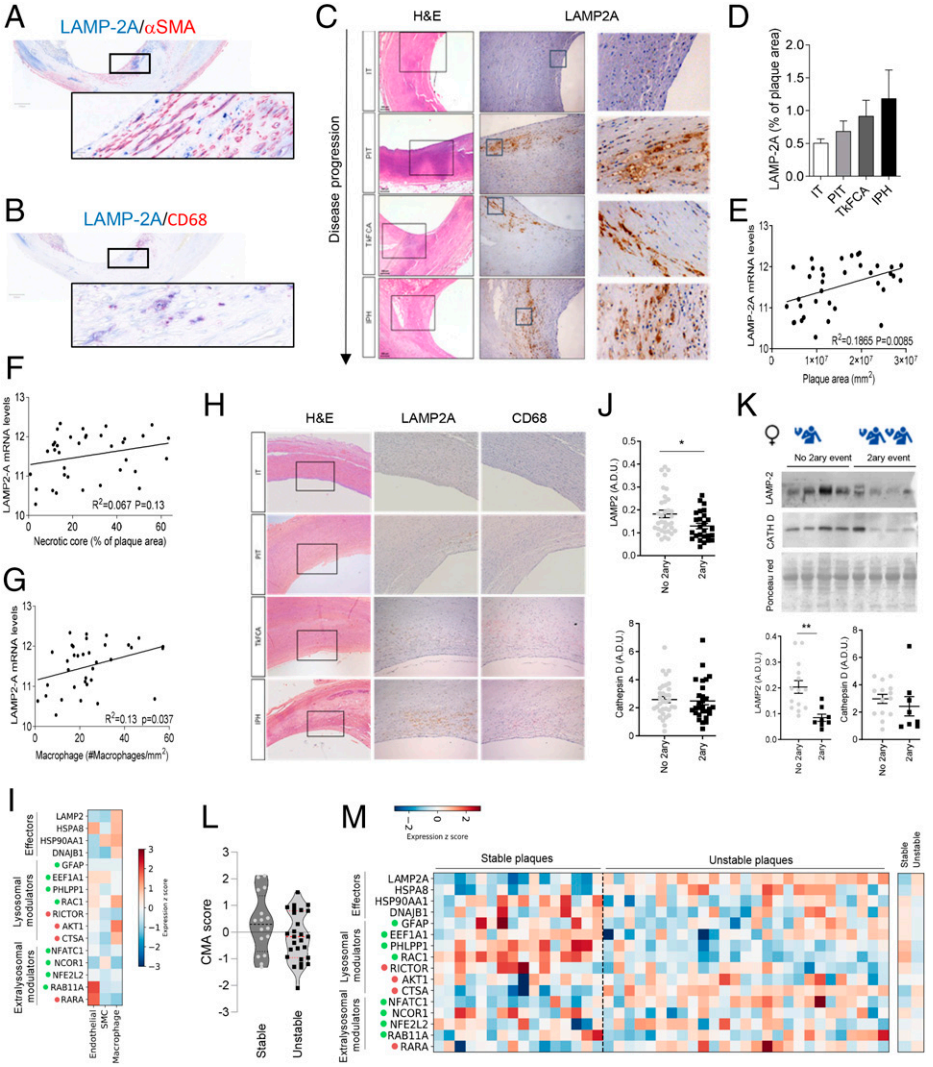

Fig. 5. CMA changes in aorta of atherosclerotic patients with disease. (*A–H*) LAMP-2A levels in different stages of carotid artery atherosclerotic plaque development sourced from asymptomatic subjects at autopsy (study 1). Representative images of the colocalization of LAMP-2A with αSMA- (*A*) and CD68- (*B*) positive cells in human atherosclerotic plaques. Representative images of H&E staining (*Left*) and LAMP-2A immunostaining (*Middle*; higher magnification, *Right*) (*C*); quantification of LAMP-2A staining intensity relative to plaque area (study 1; n = 7–12 per group) (*D*). Correlation between mRNA levels of *LAMP*-2A and plaque area (*E*), the extent of the necrotic core (*F*) and macrophage content (*G*) in carotid artery plaques from symptomatic subjects (study 2; n = 36). Comparison of immunostaining for LAMP-2A (*Middle*) and the macrophage marker CD68 (*Right*) in adjacent sections from the same patient (*H*; study 1). (*I*) Normalized expression (within each cell type) of individual components of the CMA network in scRNAseq from human coronary atherosclerotic plaques from heart transplants (study 3; n = 4). Only three major cell types are highlighted here; results for the other cell types can be found in *SI Appendix*, Fig. S6*B*. CMA network elements are organized in functional groups and colored dots indicate the effect of a given element on CMA activity (green, positive element; red, negative element). (*J* and *K*) Protein levels for LAMP2 and cathepsin D in carotid artery plaque lysates from symptomatic patients who experienced a secondary coronary event (2ary event) or not (no 2ary event) (study 4; n = 34 no 2ary event, n = 28 2ary event) subjected to immunoblot. Average and individual values in all samples independent of sex (*J*) and representative immunoblot (*Top*) and values in females only (14 no 2ary event, n = 8 2ary event) (*K*). Ponceau red is shown as loading control. (*L* and *M*) CMA activation score (*L*) calculated from normalized mRNA expression data (shown in *M*) between stable and unstable carotid artery atherosclerotic plaques (study 2). Decrease of the score indicates a predicted transcriptional inhibition of the pathway ($t41$ = 1.612, P = 0.1146). Normalized expression of individual components of the CMA network in RNAseq from stable (n = 16) and unstable atherosclerotic plaques (n = 26) (study 2). CMA network elements are organized in functional groups and colored dots are as in *I*. All data, when applicable, were tested for normal distribution using the D'Agostino and Pearson normality test. Variables that did not pass the normality test were subsequently analyzed using the Mann–Whitney *U* rank-sum test. All other variables were tested with the Student's *t* test. Individual patient values and mean ± SEM are shown. *P < 0.05 and **P < 0.01.

cathepsin D, another lysosomal marker, remained unchanged (Fig. 5 *J* and *K* and *SI Appendix*, Fig. S6 *C* and *E*). We have recently developed and validated an algorithm that allows inferring CMA activity based on the weighted averaged expression of the genes known to contribute as effectors or regulators to CMA (*SI Appendix*, Fig. S6*A*). Analysis of the CMA score using transcriptomics from patient plaques predicted a reduction of CMA activity in unstable atherosclerotic plaques when compared with stable ones (study 2; Fig. 5*L*). Deconvolution analysis highlighted an overall lower expression of most network elements, especially of positive lysosomal modulators, despite an increase of effectors (*LAMP-2A* and *HSC70*) (Fig. 5*M*). This increase in *LAMP-2A* mRNA can be interpreted as an attempt to compensate for the pronounced decrease in LAMP-2A protein levels in these patients, likely due to reduced stability of this protein, as previously observed upon persistent lipid challenges (29).

These findings support that atherosclerotic disease also associates with dysfunctional CMA in the vasculature in humans.

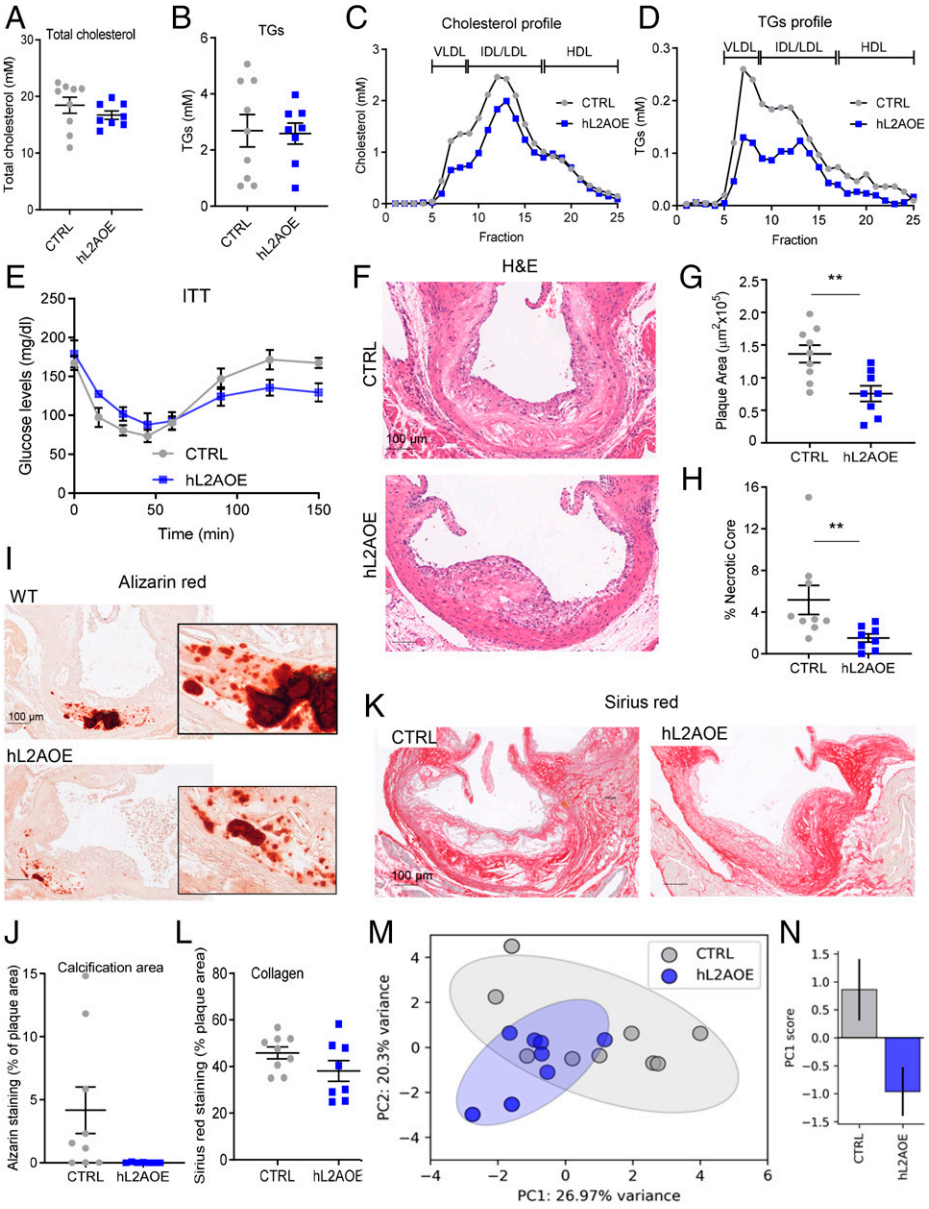

Fig. 6. Genetic up-regulation of CMA ameliorates disease in an atherosclerosis murine experimental model. (*A–D*) Circulating lipids in control mice (CTRL) and in mice systemically expressing a copy of human LAMP-2A (hL2AOE) subjected to a proatherosclerotic intervention (injected with AAV8-PCSK9 and maintained for 12 wk on WD). Circulating total cholesterol (*A*), TGs (*B*), cholesterol profile (*C*), and TG profile (*D*); $n = 9$ CTRL, $n = 8$ hL2AOE. IDL, intermediate density LDL. (*E*) Insulin tolerance test in the same mice (repeated-measures two-way ANOVA after Bonferroni's post hoc test, $F = 3.159$; $P = 0.0047$ for interaction, $F = 21.02$; $P < 0.0001$ for time, $F = 1.578$; $P = 0.098$ for genotype) in the same mice. (*F–L*) Properties of the plaques from aortas of the same mouse groups. Representative images of aortas stained for H&E (*F*), alizarin red (*I*), or sirius red (*K*) and quantification of plaque area (*G*), size of the necrotic core (*H*), calcification presence (*J*), and collagen deposition (*L*); $n = 9$ CTRL, $n = 8$ hL2AOE. (*M* and *N*) Principal-component (PC) analysis of 12 variables measured in CTRL and hL2AOE mice. Each dot represents a single animal (*M*). Ellipses are the 95% CI around the center of mass of a given experimental group. The bar plot represents mean ± SEM of the PC1 score for each experimental group (*N*); $n = 9$ CTRL, $n = 8$ hL2AOE. *Student's *t* test between CTRL and hL2AOE, $t15 = 2.152$, $P = 0.048$. Individual values and mean ± SEM are presented in all quantifications. All data were tested for normal distribution using the D'Agostino and Pearson normality test. Variables that did not pass the normality test were subsequently analyzed using the Mann–Whitney *U* rank-sum test. All other variables were tested with the Student's *t* test. **$P < 0.01$.

CMA Up-Regulation Protects against Atherosclerosis in Mice. To experimentally test the proposed protective effect of CMA activation—observed early in the disease in mice and in human plaques—and to evaluate the possible therapeutic value of CMA modulation in atherosclerosis, we directly up-regulated CMA activity in mice exposed to a proatherosclerotic challenge. To that end, we used an inducible transgenic mouse model (hL2AOE), expressing the human form of LAMP-2A (45) (*SI Appendix*, Fig. S1*E*), which we induced after the observed drop in LAMP-2A levels in early plaques (Fig. 1*E* and *SI Appendix*, Fig. S7*A*). We confirmed that weight and circulating cholesterol were indistinguishable between WT and hL2AOE mice before the treatment (*SI Appendix*, Fig. S1 *F* and *G*). After the proatherosclerotic challenge, although circulating cholesterol and TG levels were only discretely reduced, increasing CMA activity markedly decreased the fraction of both lipids in the VLDL and LDL fractions (Fig. 6 *A–D*). As anticipated, the improved lipid profile of the hL2AOE group associated with an increase in insulin sensitivity (Fig. 6*E*). The hL2AOE mice also showed a trend towards an ameliorated profile of multiple proinflammatory cytokines (i.e., PAI-1, CCL3, CCL4, and G-CSF shown in *SI Appendix*, Fig. S7 *B*, *D*, and *F*) that we found modified in the opposite direction in CMA-defective mice upon the same challenge (Fig. 2*I* and *SI Appendix*, Fig. S7

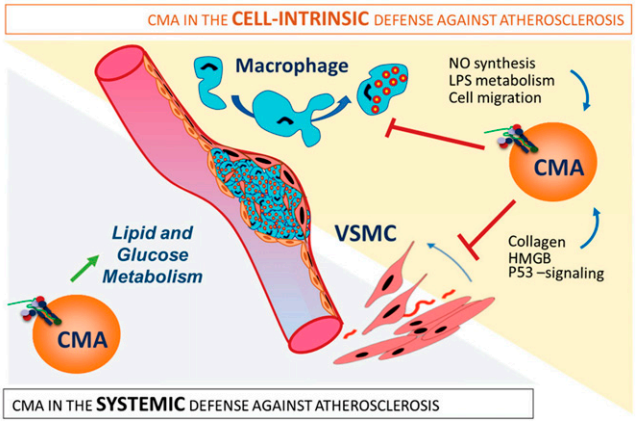

Fig. 7. CMA is part of the systemic and vascular response against proatherosclerotic insults. The protective effect of CMA against atherosclerosis results from the combination of systemic and vasculature-specific functions of CMA. (*Left*) Systemic CMA failure leads to defective lipid and glucose metabolism that increases systemic vulnerability to the metabolic syndrome. (*Right*) Defective CMA in VSMCs makes them prone to dedifferentiation because of failure to degrade proteins involved in cellular proliferation, collagen secretion, and cell death. Macrophages unable to up-regulate CMA in response to a lipotoxic stimulus acquire a more proinflammatory phenotype with higher NO levels and LPS signaling and with increased migratory capability.

C and *E*). Analysis of the atherosclerotic plaque revealed that hL2AOE mice exhibited smaller lesions with reduced necrotic cores and less calcification (Fig. 6 *F–J*), although collagen content, plaque stage, and number of VSMCs and macrophages were comparable in both groups of mice (Fig. 6 *K* and *L* and *SI Appendix*, Fig. S7 *G–J*). Principal-component analysis with 12 variable data shows that CTRL and hL2AOE mouse groups are distributed in different regions in support of these groups evolving differently upon the lipid challenge (Fig. 6 *M* and *N* and *SI Appendix*, Fig. S7 *K*).

Overall, these findings support both systemic and vascular beneficial effects of CMA up-regulation and highlight the therapeutic potential of activating CMA to prevent atherosclerotic disease progression (Fig. 7).

Discussion

In this work, we have identified a protective role for CMA against atherosclerotic disease through a combination of systemic and local effects. Fully functional CMA protects against systemic changes that promote disease progression, such as levels of circulating lipids, glucose metabolism, and immune-inflammatory response. In addition, CMA in cells in the vasculature and the plaque reduces lesion severity by preserving VSMC identity and modulating the macrophage proinflammatory phenotype. The aggravated atherosclerotic pathology observed upon CMA blockage in vivo underscores the contribution to disease progression. We propose that up-regulation of CMA is part of the organism's response to proatherogenic challenges, but that factors such as aging or sustained dietary pressure, known to inhibit CMA, reduce the efficacy of this protective mechanism. We show that genetic activation of CMA slows down disease progression in mice, supporting a potential therapeutic value of CMA up-regulation in atherosclerosis.

We favored for our study the systemic disruption of CMA to better recapitulate the overall reduced CMA activity observed in aging (32) or upon dietary lipid challenges (29). In fact, although functional CMA studies in humans are still not feasible, analysis of the expression of the CMA network genes in aortas from healthy individuals of different ages (from the Genotype–Tissue Expression [GTEx] aging database) predicted a gradual decrease with age in their overall CMA score (*SI Appendix*, Fig. S8*A*). This decrease does not seem to be related to decreased lysosomal biogenesis because while LAMP-2A expression was reduced in the older groups, expression of other lysosomal proteins such as LAMP1 increased with age (*SI Appendix*, Fig. S8*B*). scRNAseq of human aortas from the Tabula Sapiens cell atlas (46) supported a similar trend of CMA decrease with age, albeit at different rates, preferentially in macrophages and, to a lesser extent, in VSMCs (*SI Appendix*, Fig. S8 *C–F*).

As expected of a protein degradation pathway with the potential to degrade more than 45% of cytosolic proteins [those with KFERQ-like motifs (19)], the mechanisms behind the protective effect of CMA against atherosclerosis are multiple. Our findings support a systemic role for CMA in regulation of organismal metabolism. Blockage of CMA in liver leads to profound metabolic derangements due to failure to timely degrade proteins involved in glucose and lipid metabolism (26). Defective liver metabolism in the mice with systemic CMA blockage used in this study may be responsible for the abnormal cholesterol and lipoprotein profiles observed in these mice upon lipid challenge (47). Furthermore, these mice phenocopy part of the aging metabolic phenotype characterized by diminished aerobic capacity (48) and insulin resistance due to increased abdominal adiposity (38). Several systemic changes observed in the L2AKO mice [hypercholesterolemia, hypertriglyceridemia, insulin resistance, and elevated acute-phase proteins such as PAI-1 (49)] are major risk factors for atherosclerosis in humans and may contribute to the aggravating effect of CMA failure on the disease. However, our studies with isolated primary cells also highlight that part of the protective effect of CMA occurs directly at the vascular wall.

Previous studies support a relationship between autophagy, mainly macroautophagy, and atherogenesis that resembles in many aspects the one described here for CMA. Preclinical studies have shown that VSMCs up-regulate macroautophagy in response to several proatherogenic stimuli, such as lipids, proinflammatory cytokines, growth factors, and/or oxidative stress (50), whereas autophagic malfunction leads to VSMC phenotype switch and foam cell formation (15, 51, 52). In fact, mice knocked out for the essential autophagy gene ATG7 in VSMCs show impaired mitophagy and increased oxidative stress and apoptosis, all hallmarks of advanced vulnerable atherosclerotic plaques (53). A similar protective effect of macroautophagy against lipid challenges has also been described in endothelial cells (14) and macrophages (16) whereas a specific blockade of macroautophagy in macrophages in vivo leads to atherosclerosis progression (54, 55). We identified similar functions for CMA in VSMCs and macrophages in the context of proatherosclerotic stimuli to the ones described for macroautophagy. Nevertheless, these pathways are nonredundant, since blockage of only one of them is sufficient to aggravate disease progression. These findings highlight rather the complementarity between these autophagic pathways, which likely originates from their different mechanisms of action. For example, while the protective effect of macroautophagy against lipotoxicity is attained in large part through active degradation of lipid stores through lipophagy (16), we show in this work that CMA protects against lipotoxicity through regulation of the cholesterol biosynthetic pathway, by combined selective degradation of cholesterol biogenic enzymes, and of transcription factors that mediate activation of these pathways.

We also found that failure to activate CMA in response to lipid challenges is sufficient to promote a dedifferentiated activated–like phenotype in VSMCs, an essential step in

atherosclerosis etiology and development (7). In fact, the large, fibrous, and calcified plaques with extensive necrosis observed in L2AKO mice are representative of a mature stage of atherosclerosis progression that develops with aging (56) [American Heart Association classification types Vc and Vb, or fibrocalcific plaque according to Virmani et al. (12)]. We propose that impaired timely degradation by CMA of the identified intracellular signaling proteins is behind the reduced viability and failure to preserve cellular identity in CMA-defective VSMCs. For example, reduced P53 signaling can explain the higher cellular proliferation, DNA damage, and HMGB1 release and higher cell-death rates observed in CMA-deficient VSMCs upon LDL loading.

The other cellular component of the atherosclerotic plaque directly affected by changes in CMA activity is macrophages. We found quantitative and qualitative changes in the subproteome degraded by CMA during the macrophage phenotypic switch and that defective CMA under these conditions leads to an aberrant proinflammatory phenotype in these cells. Among the CMA substrates in stimulated macrophages identified in this work, proteins involved in NO synthesis, leukocyte activation and migration, cell adhesion, neutrophil degranulation, and LPS signaling have all been tightly connected with development of atherosclerosis (57, 58).

CMA is activated in response to lipotoxic stimuli, oxidative stress, and hypoxia (29–31), all coexisting conditions at the atherosclerotic plaque (4, 59, 60). We propose that the high levels of LAMP-2A identified with human plaque progression in asymptomatic subjects may be indicative of reactive CMA up-regulation, as the one observed in mice in the early stages of the proatherosclerotic challenge, to protect against later events in the human disease. In fact, a similar compensatory up-regulation, as an attempt to overcome the pathology, has also been proposed for macroautophagy in atherosclerotic patients. Ultrastructural studies in human aorta demonstrated autophagosome-like structures in atherosclerotic lesions (61), and expression of autophagy markers, such as the autophagy initiator ATG16L1, has been found increased in atherosclerotic plaques and correlates with plaque vulnerability (62). It is likely that these compensatory mechanisms, when sustained for a long period of time, may be insufficient or even no longer triggered. The reduced overall CMA score that we predicted from the transcriptional profile of advanced plaques in human aorta when compared with early plaques supports this possibility. To date, the only genetic link between CMA and cardiovascular conditions in humans is with the vacuolar cardiopathy Danon disease, where patients harbor mutations in the *LAMP2* gene (63). Genome-wide association studies have reported single-nucleotide polymorphisms for several components of the CMA network with cardiovascular and metabolic conditions (64, 65), but since those genes also participate in other cellular processes, future experimental testing will be required to explore their direct impact on CMA.

Although future studies on the status of CMA at different disease stages in patients are needed to determine the possible time frame of the efficacy of this intervention in humans, our work provides proof of concept for the therapeutic value of CMA up-regulation in atherosclerosis. Malfunctioning of both macroautophagy (55, 66, 67) and CMA (this work) has been reported in atherosclerosis disease. Interestingly, genetic up-regulation in vivo of either of them, by overexpressing the positive regulator of macroautophagy TFEB (67) or the limiting CMA component LAMP-2A (this work), successfully slows down atherosclerotic disease progression in mice. These findings and the mechanistic complementarity between both pathways provide a rationale for a possible beneficial additive effect of combinatorial therapeutics targeting both pathways.

Materials and Methods

Animal Models and Primary Cultures. All mouse models used in this work and the procedures to generate primary cultures of VSMCs and BMDMs from those models are described in detail in *SI Appendix, Methods*. All animal studies were under an animal study protocol approved by the Institutional Animal Care and Use Committee of Albert Einstein College of Medicine.

Metabolic Analysis. Plasma total cholesterol (cholesterol E; 999-02601; Wako) and TGs (L-type triglyceride M; 992-02892 and 998-02992; Wako) were assessed using standard enzymatic assays automated on the Infinite 200 PRO (Tecan). Body weight, body composition, and calorimetric data were acquired by an open-circuit indirect calorimetry system and are further described in *SI Appendix, Methods*.

Image Analysis. For immunohistochemistry, aortic roots were serially sectioned and stained with colorimetric stains or with primary antibodies and their corresponding fluorescence-conjugated secondary antibodies to visualize specific proteins. Direct Dendra fluorescence in KFERQ-Dendra2 mice was visualized using two-photon and intravital microscopy as described in detail in *SI Appendix, Methods*.

CMA Activity. CMA activity was analyzed with fluorescence reporters as described before (36, 68) or by analysis of the transcriptional changes in the genes of CMA effectors and regulators (CMA network) using the CMA score algorithm previously described and validated in ref. 69.

Data Availability. The microarray raw data reported in this article have been deposited in the Gene Expression Omnibus (accession no. GSE143162) (70); other datasets were retrieved from public repositories (71–74).

ACKNOWLEDGMENTS. We thank Trea Streefland (Leiden University Medical Center) for her assistance with generating the lipid profiles, and Jacques Debets and Clairy Dinjens (Maastricht University Medical Center) for assistance with sectioning and immunohistochemistry. The GTEx Project used for the calculation of CMA scores was supported by the Common Fund of the Office of the Director of the NIH, and the Tabula Sapiens Project, used for the same purpose, was supported by Grant 2019-203354 from the Chan Zuckerberg Initiative DAF. This work was supported by NIH Grants AG021904 and DK098408 (to A.M.C.) and AG031782 (to A.M.C., R.S., J.J.B.-C., and F.M.), the Leducq Foundation Network (A15CVD04 to A.M.C. and J.C.S.), and a Dr. Dekker Senior Postdoc Fellowship from the Dutch Heart Foundation (2016T060 to J.C.S.). J.M.-M. was supported by a postdoctoral fellowship from the American Heart Association (17POST33650088), A.M.-S. by a Ramon Areces Postdoctoral Fellowship, and G.J.K. by TGT32GM007288 and T32GM007491.

Author affiliations: [a]Department of Development and Molecular Biology, Albert Einstein College of Medicine, Bronx, NY 10461; [b]Institute for Aging Studies, Albert Einstein College of Medicine, Bronx, NY 10461; [c]Department of Pathology, Cardiovascular Research Institute Maastricht, Maastricht University Medical Center, 6229 HX Maastricht, The Netherlands; [d]Institute of Experimental Medicine and Systems Biology, Faculty of Medicine, RWTH Aachen University, 52074 Aachen, Germany; [e]Department of Medicine, Albert Einstein College of Medicine, Bronx, NY 10461; [f]School for Oncology and Developmental Biology (GROW), Maastricht University Medical Center, 6229 HX Maastricht, The Netherlands; [g]Department of Medical Biochemistry, Experimental Vascular Biology, Amsterdam University Medical Centers, University of Amsterdam, 1081 HV Amsterdam, The Netherlands; [h]Institute for Molecular Cardiovascular Research, RWTH Aachen University, 52074 Aachen, Germany; [i]Centre for Cardiovascular Science, University of Edinburgh, Edinburgh EH16 4TJ, United Kingdom; [j]Division of Hematology and Medical Oncology, Department of Medicine, Icahn School of Medicine at Mount Sinai, New York, NY 10029; [k]Department of Pathology, Albert Einstein College of Medicine, Bronx, NY 10461; [l]Section of Endocrinology, Department of Internal Medicine, Leiden University Medical Center, 2333 ZA Leiden, The Netherlands; [m]Einthoven Laboratory for Experimental Vascular Medicine, Leiden University Medical Center, 2333 ZA Leiden, The Netherlands; and [n]Experimental Cardiology Laboratory, Department of Cardiology, University Medical Center Utrecht, 3584 CX Utrecht, The Netherlands

Author contributions: J.M.-M., N.E.S.S., J.C.S., and A.M.C. designed research; J.M.-M., J.d.B., K.v.K., D.F.R.-B., A.D., I.T., A.M.-S., M.J.J.G., B.S., S.K., S.T., H.J., J.J.B.-C., F.M., R.S., and G.P. performed research; I.T., E.A.L.B., I.M., A.H.B., P.C.N.R., J.F.P.B., and G.P. contributed new reagents/analytic tools; J.M.-M., J.d.B., K.v.K., A.D., A.M.-S., B.S., S.K., M.B., G.J.K., I.M., H.J., J.J.B.-C., F.M., P.C.N.R., J.C.S., and A.M.C. analyzed data; and J.M.-M., J.C.S., and A.M.C. wrote the paper.

Reviewers: P.B., University of California, Los Angeles; and T.F., University of Pittsburgh.

1. S. S. Virani *et al.*; American Heart Association Council on Epidemiology and Prevention Statistics Committee and Stroke Statistics Subcommittee, Heart disease and stroke statistics–2021 update: A report from the American Heart Association. *Circulation* **143**, e254–e743 (2021).
2. E. J. Benjamin *et al.*; American Heart Association Statistics Committee and Stroke Statistics Subcommittee, Heart disease and stroke statistics–2017 update: A report from the American Heart Association. *Circulation* **135**, e146–e603 (2017).
3. P. Libby, The changing landscape of atherosclerosis. *Nature* **592**, 524–533 (2021).
4. I. Tabas, K. J. Williams, J. Borén, Subendothelial lipoprotein retention as the initiating process in atherosclerosis: Update and therapeutic implications. *Circulation* **116**, 1832–1844 (2007).
5. K. J. Moore, I. Tabas, Macrophages in the pathogenesis of atherosclerosis. *Cell* **145**, 341–355 (2011).
6. Y. Vengrenyuk *et al.*, Cholesterol loading reprograms the microRNA-143/145-myocardin axis to convert aortic smooth muscle cells to a dysfunctional macrophage-like phenotype. *Arterioscler. Thromb. Vasc. Biol.* **35**, 535–546 (2015).
7. M. R. Bennett, S. Sinha, G. K. Owens, Vascular smooth muscle cells in atherosclerosis. *Circ. Res.* **118**, 692–702 (2016).
8. R. C. Wirka *et al.*, Atheroprotective roles of smooth muscle cell phenotypic modulation and the TCF21 disease gene as revealed by single-cell analysis. *Nat. Med.* **25**, 1280 (2019).
9. P. Libby, Vascular biology of atherosclerosis: Overview and state of the art. *Am. J. Cardiol.* **91** (3A), 3A–6A (2003).
10. M. J. Mitchinson, S. J. Hardwick, M. R. Bennett, Cell death in atherosclerotic plaques. *Curr. Opin. Lipidol.* **7**, 324–329 (1996).
11. D. Proudfoot *et al.*, Apoptosis regulates human vascular calcification in vitro: Evidence for initiation of vascular calcification by apoptotic bodies. *Circ. Res.* **87**, 1055–1062 (2000).
12. R. Virmani, F. D. Kolodgie, A. P. Burke, A. Farb, S. M. Schwartz, Lessons from sudden coronary death: A comprehensive morphological classification scheme for atherosclerotic lesions. *Arterioscler. Thromb. Vasc. Biol.* **20**, 1262–1275 (2000).
13. N. Mizushima, M. Komatsu, Autophagy: Renovation of cells and tissues. *Cell* **147**, 728–741 (2011).
14. K. Torisu *et al.*, Intact endothelial autophagy is required to maintain vascular lipid homeostasis. *Aging Cell* **15**, 187–191 (2016).
15. M. O. Grootaert *et al.*, Defective autophagy in vascular smooth muscle cells accelerates senescence and promotes neointima formation and atherogenesis. *Autophagy* **11**, 2014–2032 (2015).
16. M. Ouimet *et al.*, Autophagy regulates cholesterol efflux from macrophage foam cells via lysosomal acid lipase. *Cell Metab.* **13**, 655–667 (2011).
17. J. M. Henderson, C. Weber, D. Santovito, Beyond self-recycling: Cell-specific role of autophagy in atherosclerosis. *Cells* **10**, 625 (2021).
18. J. F. Dice, Peptide sequences that target cytosolic proteins for lysosomal proteolysis. *Trends Biochem. Sci.* **15**, 305–309 (1990).
19. P. Kirchner *et al.*, Proteome-wide analysis of chaperone-mediated autophagy targeting motifs. *PLoS Biol.* **17**, e3000301 (2019).
20. H. L. Chiang, S. R. Terlecky, C. P. Plant, J. F. Dice, A role for a 70-kilodalton heat shock protein in lysosomal degradation of intracellular proteins. *Science* **246**, 382–385 (1989).
21. A. M. Cuervo, J. F. Dice, A receptor for the selective uptake and degradation of proteins by lysosomes. *Science* **273**, 501–503 (1996).
22. U. Bandyopadhyay, S. Kaushik, L. Varticovski, A. M. Cuervo, The chaperone-mediated autophagy receptor organizes in dynamic protein complexes at the lysosomal membrane. *Mol. Cell. Biol.* **28**, 5747–5763 (2008).
23. F. A. Agarraberes, S. R. Terlecky, J. F. Dice, An intralysosomal hsp70 is required for a selective pathway of lysosomal protein degradation. *J. Cell Biol.* **137**, 825–834 (1997).
24. N. Salvador, C. Aguado, M. Horst, E. Knecht, Import of a cytosolic protein into lysosomes by chaperone-mediated autophagy depends on its folding state. *J. Biol. Chem.* **275**, 27447–27456 (2000).
25. J. L. Schneider, Y. Suh, A. M. Cuervo, Deficient chaperone-mediated autophagy in liver leads to metabolic dysregulation. *Cell Metab.* **20**, 417–432 (2014).
26. S. Kaushik, A. M. Cuervo, Degradation of lipid droplet-associated proteins by chaperone-mediated autophagy facilitates lipolysis. *Nat. Cell Biol.* **17**, 759–770 (2015).
27. R. Valdor *et al.*, Chaperone-mediated autophagy regulates T cell responses through targeted degradation of negative regulators of T cell activation. *Nat. Immunol.* **15**, 1046–1054 (2014).
28. A. M. Cuervo, H. Hildebrand, E. M. Bomhard, J. F. Dice, Direct lysosomal uptake of alpha 2-microglobulin contributes to chemically induced nephropathy. *Kidney Int.* **55**, 529–545 (1999).
29. J. A. Rodriguez-Navarro *et al.*, Inhibitory effect of dietary lipids on chaperone-mediated autophagy. *Proc. Natl. Acad. Sci. U.S.A.* **109**, E705–E714 (2012).
30. R. Kiffin, C. Christian, E. Knecht, A. M. Cuervo, Activation of chaperone-mediated autophagy during oxidative stress. *Mol. Biol. Cell* **15**, 4829–4840 (2004).
31. E. Dohi *et al.*, Hypoxic stress activates chaperone-mediated autophagy and modulates neuronal cell survival. *Neurochem. Int.* **60**, 431–442 (2012).
32. A. M. Cuervo, J. F. Dice, Age-related decline in chaperone-mediated autophagy. *J. Biol. Chem.* **275**, 31505–31513 (2000).
33. R. Kiffin *et al.*, Altered dynamics of the lysosomal receptor for chaperone-mediated autophagy with age. *J. Cell Sci.* **120**, 782–791 (2007).
34. S. Sooparb, S. R. Price, J. Shaoguang, H. A. Franch, Suppression of chaperone-mediated autophagy in the renal cortex during acute diabetes mellitus. *Kidney Int.* **65**, 2135–2144 (2004).
35. J. Madrigal-Matute, L. Scorrano, J. Sadoshima, Leducq Network: Modulating autophagy to treat cardiovascular disease. *Circ. Res.* **123**, 323–325 (2018).
36. S. Dong *et al.*, Monitoring spatiotemporal changes in chaperone-mediated autophagy in vivo. *Nat. Commun.* **11**, 645 (2020).
37. J. L. Schneider *et al.*, Loss of hepatic chaperone-mediated autophagy accelerates proteostasis failure in aging. *Aging Cell* **14**, 249–264 (2015).
38. W. M. Kohrt *et al.*, Insulin resistance in aging is related to abdominal obesity. *Diabetes* **42**, 273–281 (1993).
39. Z. Tan *et al.*, P53 promotes retinoid acid-induced smooth muscle cell differentiation by targeting myocardin. *Stem Cells Dev.* **27**, 534–544 (2018).
40. A. R. Davalos *et al.*, p53-dependent release of Alarmin HMGB1 is a central mediator of senescent phenotypes. *J. Cell Biol.* **201**, 613–629 (2013).
41. M. Stros, E. Muselíková-Polanská, S. Pospísilová, F. Strauss, High-affinity binding of tumor-suppressor protein p53 and HMGB1 to hemicatenated DNA loops. *Biochemistry* **43**, 7215–7225 (2004).
42. M. Parra, M. Jardí, M. Koziczak, Y. Nagamine, P. Muñoz-Cánoves, p53 phosphorylation at serine 15 is required for transcriptional induction of the plasminogen activator inhibitor-1 (PAI-1) gene by the alkylating agent *N*-methyl-*N*′-nitro-*N*-nitrosoguanidine. *J. Biol. Chem.* **276**, 36303–36310 (2001).
43. H. Jin *et al.*, Integrative multiomics analysis of human atherosclerosis reveals a serum response factor-driven network associated with intraplaque hemorrhage. *Clin. Transl. Med.* **11**, e458 (2021).
44. W. E. Hellings *et al.*, Composition of carotid atherosclerotic plaque is associated with cardiovascular outcome. *Circulation* **121**, 1941–1950 (2010).
45. S. Dong *et al.*, Chaperone-mediated autophagy sustains haematopoietic stem-cell function. *Nature* **591**, 117–123 (2021).
46. The Tabula Sapiens Consortium, S. R. Quake, The Tabula Sapiens: A multiple organ single cell transcriptomic atlas of humans. bioRxiv [Preprint] (2021). https://doi.org/10.1101/2021.07.19.452956 (Accessed 15 January 2022).
47. J. L. Goldstein, M. S. Brown, A century of cholesterol and coronaries: From plaques to genes to statins. *Cell* **161**, 161–172 (2015).
48. J. L. Fleg *et al.*, Accelerated longitudinal decline of aerobic capacity in healthy older adults. *Circulation* **112**, 674–682 (2005).
49. A. Festa *et al.*; The Insulin Resistance Atherosclerosis Study (IRAS), Relative contribution of insulin and its precursors to fibrinogen and PAI-1 in a large population with different states of glucose tolerance. *Arterioscler. Thromb. Vasc. Biol.* **19**, 562–568 (1999).
50. M. O. J. Grootaert *et al.*, Vascular smooth muscle cell death, autophagy and senescence in atherosclerosis. *Cardiovasc. Res.* **114**, 622–634 (2018).
51. S. Pi *et al.*, The P2RY12 receptor promotes VSMC-derived foam cell formation by inhibiting autophagy in advanced atherosclerosis. *Autophagy* **17**, 980–1000 (2021).
52. J. K. Salabei *et al.*, PDGF-mediated autophagy regulates vascular smooth muscle cell phenotype and resistance to oxidative stress. *Biochem. J.* **451**, 375–388 (2013).
53. H. Nahapetyan *et al.*, Altered mitochondrial quality control in Atg7-deficient VSMCs promotes enhanced apoptosis and is linked to unstable atherosclerotic plaque phenotype. *Cell Death Dis.* **10**, 119 (2019).
54. X. Liao *et al.*, Macrophage autophagy plays a protective role in advanced atherosclerosis. *Cell Metab.* **15**, 545–553 (2012).
55. B. Razani *et al.*, Autophagy links inflammasomes to atherosclerotic progression. *Cell Metab.* **15**, 534–544 (2012).
56. G. W. van Lammeren *et al.*, Atherosclerotic plaque vulnerability as an explanation for the increased risk of stroke in elderly undergoing carotid artery stenting. *Stroke* **42**, 2550–2555 (2011).
57. M. E. Burleigh *et al.*, Cyclooxygenase-2 promotes early atherosclerotic lesion formation in LDL receptor-deficient mice. *Circulation* **105**, 1816–1823 (2002).
58. P. A. Detmers *et al.*, Deficiency in inducible nitric oxide synthase results in reduced atherosclerosis in apolipoprotein E-deficient mice. *J. Immunol.* **165**, 3430–3435 (2000).
59. J. L. Martin-Ventura *et al.*, Erythrocytes, leukocytes and platelets as a source of oxidative stress in chronic vascular diseases: Detoxifying mechanisms and potential therapeutic options. *Thromb. Haemost.* **108**, 435–442 (2012).
60. J. C. Sluimer *et al.*, Hypoxia, hypoxia-inducible transcription factor, and macrophages in human atherosclerotic plaques are correlated with intraplaque angiogenesis. *J. Am. Coll. Cardiol.* **51**, 1258–1265 (2008).
61. I. Perrotta, The use of electron microscopy for the detection of autophagy in human atherosclerosis. *Micron* **50**, 7–13 (2013).
62. J. Magné *et al.*, ATG16L1 expression in carotid atherosclerotic plaques is associated with plaque vulnerability. *Arterioscler. Thromb. Vasc. Biol.* **35**, 1226–1235 (2015).
63. I. Nishino *et al.*, Primary LAMP-2 deficiency causes X-linked vacuolar cardiomyopathy and myopathy (Danon disease). *Nature* **406**, 906–910 (2000).
64. D. Klarin *et al.*; Global Lipids Genetics Consortium; Myocardial Infarction Genetics (MIGen) Consortium; Geisinger-Regeneron DiscovEHR Collaboration; VA Million Veteran Program, Genetics of blood lipids among ~300,000 multi-ethnic participants of the Million Veteran Program. *Nat. Genet.* **50**, 1514–1523 (2018).
65. T. G. Richardson *et al.*, Evaluating the relationship between circulating lipoprotein lipids and apolipoproteins with risk of coronary heart disease: A multivariable Mendelian randomisation analysis. *PLoS Med.* **17**, e1003062 (2020).
66. I. Sergin *et al.*, Inclusion bodies enriched for p62 and polyubiquitinated proteins in macrophages protect against atherosclerosis. *Sci. Signal.* **9**, ra2 (2016).
67. I. Sergin *et al.*, Exploiting macrophage autophagy-lysosomal biogenesis as a therapy for atherosclerosis. *Nat. Commun.* **8**, 15750 (2017).
68. H. Koga, M. Martinez-Vicente, F. Macian, V. V. Verkhusha, A. M. Cuervo, A photoconvertible fluorescent reporter to track chaperone-mediated autophagy. *Nat. Commun.* **2**, 386 (2011).
69. M. Bourdenx *et al.*, Chaperone-mediated autophagy prevents collapse of the neuronal metastable proteome. *Cell* **184**, 2696–2714.e25 (2021).
70. J. Madrigal-Matute *et al.*, Transcriptome analysis of vascular smooth muscle cells from mice deficient for chaperone-mediated autophagy. Gene Expression Omnibus. https://www.ncbi.nlm.nih.gov/geo/query/acc.cgi?acc=GSE143162. Deposited 6 January 2020.
71. R. C. Wirka et al., Data from "Single cell analysis of smooth muscle cell phenotypic modulation in vivo during disease in mice and humans." Gene Expression Omnibus. https://www.ncbi.nlm.nih.gov/geo/query/acc.cgi?acc=GSE131780. Accessed 14 December 2020.
72. J. H. Goossens *et al.*, Human microarray stable and unstable plaques. Gene Expression Omnibus. https://www.ncbi.nlm.nih.gov/geo/query/acc.cgi?acc=GSE163154. Accessed 14 December 2020.
73. The Tabula Sapiens, Tabula Sapiens Portal. Dataset. https://tabula-sapiens-portal.ds.czbiohub.org. Accessed 15 January 2022.
74. The Genotype-Tissue Expression (GTEx), GTEx Multi Gene Query. https://gtexportal.org/home/multiGeneQueryPage. Accessed 15 January 2022.ed